ResearchGate

See discussions, stats, and author profiles for this publication at: https://www.researchgate.net/publication/260617407

Reply to the Comment on ``Are Vibrationally Excited Molecules a Clue for the O3Deficit Problem and HOxDilemma in the Middle Atmosphere?''

ARTICLE *in* THE JOURNAL OF PHYSICAL CHEMISTRY A · MARCH 2005

Impact Factor: 2.69 · DOI: 10.1021/jp040745h

CITATIONS
13

READS
25

1 AUTHOR:

Antonio J. C. Varandas
University of Coimbra
382 PUBLICATIONS **6,727** CITATIONS

SEE PROFILE

Available from: Antonio J. C. Varandas
Retrieved on: 22 January 2016

Are Vibrationally Excited Molecules a Clue for the "O_3 Deficit Problem" and "HO_x Dilemma" in the Middle Atmosphere?

A. J. C. Varandas*

Departamento de Química, Universidade de Coimbra, 3004-535 Coimbra, Portugal

Received: August 6, 2003; In Final Form: October 8, 2003

Stretched oxygen and odd hydrogen species are suggested to offer a clue to explain the so-called "ozone deficit problem" and "HO_x dilemma" in the upper stratosphere and mesosphere under conditions of local thermodynamic disequilibrium.

1. Introduction

Ozone related problems have so intensely been highlighted in the media that "ozone hole" seems a term mated for life. Densest at an altitude of[1,2] 25−30 km, the ozone layer that envelopes the planet extends to the mesosphere (85 km) where its chemistry attains greatest simplicity. Paradoxically, it is there that some mysteries remain unfold. It is an attempt to their elucidation that we report in the present work.

Ozone is believed to form in the same way througout the atmosphere: oxygen atoms are produced by photodissociation of O_2 with a photon of frequency ν

$$O_2 + h\nu \rightarrow 2O \tag{1}$$

binding quickly with an unsplit O_2 to form O_3; h is Planck's constant. Thus, the term odd oxygen is used to imply either an O or O_3. Conversely, ozone destruction varies with location, being most complicated over the poles where winds, ice clouds, and low temperatures help various forms of halogen and nitrogen compounds to destroy O_3. However, in the upper stratosphere and mesosphere, the ozone chemistry is mostly controlled by catalytic reactions involving odd hydrogen HO_x species (x = 0, hydrogen; 1, hydroxyl; 2, hydroperoxyl):

$$O + OH \rightarrow H + O_2 \tag{2}$$

$$O + HO_2 \rightarrow OH + O_2 \tag{3}$$

with the ultimate source of HO_x radicals being the photochemical destruction of water. Below 60 km this occurs via

$$O(^1D) + H_2O \rightarrow 2OH \tag{4}$$

with $O(^1D)$ atoms being formed from the photolysis of ozone at wavelengths shorter than about 325 nm and above that altitude by photolysis of H_2O mainly through absorption of Lyman α radiation. [This photodissociation channel, known as the singlet channel, contributes ∼90% to give $O(^1D) + O_2(a^1\Delta)$ while the triplet channel contributes the remaining 10% to yield $O(^3P) + O_2(X^3\Sigma_g^-, v)$. As usual,[3,4] v or $\boldsymbol{v}$ (for a triatomic or larger molecule, this is a collective variable of all vibrational quantum numbers) identifies heretofore a species in a highly vibrationally excited state.] In turn, the primary sink of HO_x (OH and HO_2) is the reaction

$$OH + HO_2 \rightarrow O_2 + H_2O \tag{5}$$

Despite such a simplicity, in the 1980s, models underpredicted the amount of O_3 at such altitudes by 50−60%, a shortcoming known as the "ozone deficit problem".

By the middle 1990s, steady efforts in observation and theory (Crutzen et al.[5] found a surplus, others[6,7,8] found a deficiency, and novel ozone sources were proposed[3]) were giving the impression that the "ozone deficit problem" had been clarified. However, difficulties were known to persist[3] in the upper stratosphere and mesosphere, while a so-called[9] "HO_x dilemma" was about to emerge. In fact, as briefly surveyed next, standard chemical models could not give a complete understanding of the HO_x chemistry in the middle atmosphere. Summers et al.[10] reported measurements of OH between 50 and 80 km that were about 25−30% lower than expected based on standard photochemical theory. By noting a coincidence between maxima in measured OH concentrations (as usual, this will be denoted by square brackets embracing the chemical species, in this case [OH]) and the ozone observations, they suggested that a good correspondence between the ozone production and destruction rates could be obtained if a downward revision in the rate constant of reaction 3 could be done. However, the proposed downward revision by 50 to 70% lacks support both from theoretical[11−13] and recommended[14] data while leading to large underestimates of the observed abundances[6] of OH and HO_2. In turn, Sandor and Clancy[15] found that ground-based microwave measurements of HO_2 concentrations at 50−80 km altitudes were 23−47% higher than photochemical model values at mid day, agree with model values at 0900 local time, and exceed model mixing ratios by 70−100% immediately after sunset. Because neither of such studies obtained simultaneous measurements of [OH] and [HO_2], it is difficult to discern the factors that cause the imbalance. Such a difficulty was overcome by Jucks et al.,[16] who have reported balloon-borne simultaneous measurements of both species in the middle and upper stratosphere as well as of H_2O and O_3 using a far infrared spectrometer (FIRS-2). Based on a photochemical model, they have concluded that (a) the measured [OH] agrees reasonably well with, and measured [HO_2] is significantly higher than, values calculated using standard kinetic parameters for altitudes between 40 and 50 km; (b) modifications to both the partitioning

* To whom correspondence should be addressed. E-mail: varandas@qtvs1.qui.uc.pt.

10.1021/jp036321p CCC: $27.50 © 2004 American Chemical Society
Published on Web 01/29/2004

of HO_x and the balance of production and loss of HO_x were necessary to explain the observed $[HO_2]/[OH]$ ratio and abundance of HO_x; (c) the changes to reaction rates proposed by Summers et al.[10] and Sandor and Clancy[15] to explain their observations were inconsistent with the simultaneous FIRS-2 observations of [OH] and $[HO_2]$. More specifically, Jucks et al.[16] found that the measured [OH] and $[HO_2]$ above 38 km could best be modeled by calculations that used a 25% reduction in the ratio of the rate constants for reactions 2 and 3 as well as either a 25% reduction of the rate constant of reaction 5 or a 25% increase in HO_x production. With such sets of parameters, their agreement for [OH] was similar to that previously reported near 40 km by Pickett and Peterson,[17] whereas the discrepancy for $[HO_2]$ followed the pattern reported by Sandor and Clancy[15] for altitudes above 50 km. Despite the fact that the proposed changes were consistent with the uncertainties in the recommended rate constants, Jucks et al.[16] raised also the possibility that there could be "an undocumented reaction that converts OH to HO_2", although they judged such a reaction to be unlikely "given the extensive laboratory studies of OH reactions over the past two decades". Moreover, and most importantly, they emphasized that their modifications of the standard kinetics parameters "could not lead to a resolution of the long-standing 'ozone deficit problem' above 45 km". More recently, from the MAHRSI (middle atmosphere high-resolution spectrograph investigation) measurements in August 1997 at latitudes ranging between 42 and 58°, Conway et al.[9] concluded that mesospheric OH densities are 25−35% lower than predicted by standard photochemical theory but also observed that the OH density increases rapidly below 50 km being at 43 km larger than predicted by standard theory. Quantitatively, the deficit of predicted OH density relative to observation at the maximum of the vertical distribution amounts to about 20%.[9,18] Clearly, standard photochemical theory is unable to explain both observations, which is a genuine manifestation of the "HO_x dilemma".

Because N_2 (the major constituent of the atmosphere) would appear to have an innocuous role, at least to a first approximation, the "ozone deficit problem" and "HO_x dilemma" should be interrelated. Within this spirit, we have made an attempt to reconcile the observations and laboratory measurements with theory, by proposing[4,19] new mechanisms for ozone formation based on stretched odd hydrogen and oxygen molecules under the hypothesis of local thermodynamic disequilibrium (LTD). Indeed, whereas rotational relaxation of most molecules is known to occur on the 1−10 collision time scale, vibrational relaxation of diatomic molecules require about 10^5-10^6 collisions (larger polyatomics such as HO_2 relax within 10^2-10^3 collisions). This is well-known from studies (ref 20, and references therein) of polyatomic molecules during thermal decomposition or recombination, an issue that will be further examined later in relation to the problems discussed in the present work. Note that such vibrationally excited species are abundant in the stratosphere and mesosphere: $O_2(v)$ is primarily produced from ozone photodissociation; $OH(v)$ is mostly formed via the reaction[21] $H + O_3 \rightarrow OH(X\ ^2\Pi, v \leq 9) + O_2$. Indeed, as discussed below, such a proposition seems to help in resolving simultaneously both the "ozone deficit" and "HO_x dilemma".

Theoretically, the study of the elementary chemical reactions involved in the O_x and HO_x mechanisms as well as in other mechanisms that may provide a complete understanding of the chemical composition of the atmosphere is very demanding. In fact, the relevant species involved possess in general an open shell electronic structure, and hence, nonadiabatic effects are likely to be of relevance in describing their collision dynamics. For example, the group of Wodtke[22] has shown experimental evidence of spin−orbit coupling in highly vibrational excited O_2, suggesting that studies of vibrational to electronic energy transfer may be of relevance when the relevant potential energy surfaces for the O_4 system become available.[23] In turn, conical intersections for $HO_2(^2A'')$ are well established,[24−27] implying that nonadiabatic quantum dynamics may ultimately be required for studying the $H + O_2$ reaction or at least generalized Born−Oppenheimer calculations that account for the so-called geometric phase effect.[28−32] Although the above list could be made much longer, the modeling of the atmosphere within the Born−Oppenheimer approximation is in itself so challenging that the problem of fully accounting for nonadiabaticity in this field will probably be beyond reach for some years to come.

The paper is organized as follow. In section 2 we summarize the proposed mechanisms, whereas the results are presented in section 3. These include energy distributions in section 3.1 and the possible implications in the HO_2/OH partition and O_3 production in sections 3.2 and 3.3, respectively. The conclusions are in section 4.

2. Novel Mechanisms

The simplest mechanism (this is known as the $y = 0$ mechanism if odd hydrogen species are written as HO_{y+3}; the odd hydrogen supermolecule is in this case HO_3) assumes the form[4]

$$3[H + O_3 \rightarrow OH(v') + O_2] \quad (6)$$

$$3[O_3 + h\nu \rightarrow O_2(v'') + O] \quad (7)$$

$$OH(v') + O_2(v'') \rightarrow O_3 + H \quad (8)$$

$$OH(v') + O_2(v'') \rightarrow O_2 + O + H \quad (9)$$

$$OH(v') + O_2(v'') \rightarrow OH + 2O \quad (10)$$

$$6[O + O_2 + M \rightarrow O_3 + M] \quad (11)$$

$$\text{Net: } H + 2O_2 + 3h\nu \rightarrow O_3 + OH \quad (12)$$

which shows that OH formation is enhanced at the expenses of hydrogen atoms; M is a third body. However, [H] is rather small up to 40 km reaching at 55−60 km the value of [OH] reported in the literature,[1] which attains its maximum value close to 65 km (see ref 9 and section 3.2 for a somewhat different representation). The $y = 0$ and 1 mechanisms should therefore be considered together in the upper stratosphere and mesosphere (given the relatively small rate constant[14,33,34] of the $HO_2 + O_3$ reaction, we ignore at this stage the mechanism involving $y = 2$).

The $y = 1$ mechanism[4] starts with

$$OH + O_3 \rightarrow HO_2(v) + O_2 \quad (13)$$

which is the main source[1,2] of HO_2 in the middle atmosphere, being its net result

$$OH + 2O_2 + 3h\nu \rightarrow O_3 + HO_2 \quad (14)$$

In turn, the net result of the compound $y = (0, 1)$ mechanism is

$$H + 4O_2 + 6h\nu \rightarrow 2O_3 + HO_2 \quad (15)$$

which suggests that, relative to standard photochemical theory, HO_2 formation is favored at the altitudes of concern in the present work. The above results seem then to corroborate the observation that the measured $[HO_2]$ are significantly higher[15,16] and [OH] lower[9,10] than predicted by standard photochemical theory (see also section 3.2).

To emphasize its role as an ozone source, the $y = (0, 1)$ mechanism may alternatively be formulated as the following cycle:

$$3[H + O_3 \rightarrow OH(v') + O_2] \quad (16)$$

$$OH + O_3 \rightarrow H + O_2(v) + O_2 \quad (17)$$

$$4[O_3 + h\nu \rightarrow O_2(v'') + O] \quad (18)$$

$$OH(v') + O_2(v'') \rightarrow O_3 + H \quad (19)$$

$$OH(v') + O_2(v'') \rightarrow O_2 + O + H \quad (20)$$

$$OH(v') + O_2(v'') \rightarrow OH + 2O \quad (21)$$

$$O_2(v) + O_2(v'') \rightarrow O_3 + O \quad (22)$$

$$8[O + O_2 + M \rightarrow O_3 + M] \quad (23)$$

$$\text{Net: } 3O_2 + 4h\nu \rightarrow 2O_3 \quad (24)$$

Note that both the above formulations rely on elementary processes that were the subject of extensive dynamics calculations in our group.[4,11,19,35−38] Note further that Miller et al.[3] proposed a mechanism for ozone production based on the reaction

$$O_2(v'') + O_2 \rightarrow O_3 + O \quad (25)$$

Such a mechanism was motivated by measurements of the total depletion rate of $O_2(v'')$ in collisions with O_2 which have shown the opening of a so-called "dark channel" for $v \geq 25$ that is different than purely vibrational relaxation and chemical reaction. Because the bimodal distribution for ozone photodissociation leading to $O_2(v)$ has a maximum at $v = 27$, such a channel could then be of relevance to explain the novel mechanisms related to the "ozone deficit problem" and "HO_x dilemma". Unfortunately, experiment has failed to provide direct evidence showing that O_3 is formed,[39,40] with the caveat extending also to the available dynamics studies.[41−49] It should be noted that these theoretical dynamics studies employed either our own single-valued global potential energy surface[50] obtained from the DMBE (double many-body expansion[51−53]) method for ground triplet O_4 or reduced-dimensionality single-valued ab initio surfaces,[41,47] and hence the relevance of nonadiabatic processes in explaining the above experimental results remains an open question.[22,49] However, dynamics studies[4,11] have shown that odd oxygen can be formed if the O_x mechanism is reformulated to involve two vibrationally excited molecules, although this second-order process can occur only if two such species have a chance of colliding with each other.

For the novel HO_x mechanisms to deserve credit, it is of key importance to know the rate constants at which $OH(v')$ and $O_2(v'')$ vibrationally relax.[38,48,54−59,60] Theoretically, this requires potential energy surfaces with an accurate description of the long-range interactions, because we are interested in low-temperature regimes. Although DMBE[51−53] surfaces hope for such an accuracy, such a requirement can hardly be achieved especially in the case of molecule−molecule interactions. In fact, even more important than the rate constants is perhaps to know the associated (reactive versus relaxation) rates. For this, it is necessary to know the concentrations of the various species and the involved state-specific rate constants and vibrational−rotational micropopulations. This is a very demanding issue mainly because such species are not generally observable,[61] a topic which will be addressed further in section 3.1.

3. Results and Discussion

3.1. Energy Distributions. If thermal equilibration exists, the Boltzmann distribution at a particular temperature will be applicable. On the other hand, the nascent distributions [e.g., of $O_2(v')$ in the O_3 photolysis or $OH(v')$ in reaction 16] are generally far from Boltzmann-type, being fairly well understood at present. Clearly, such nascent distributions can be modified by nonreactive (and reactive) processes in collisions with O_2 and N_2, which are by far the major constituents of the atmosphere, and eventually with other minor atmospheric constituents. This leads to the distribution actually present in the environment: steady-state distribution. Although this cannot be anticipated prior to considering the environment in its full photochemical complexity, a first approximation may be obtained by assuming that vibrationally cold O_2 is the dominant quencher. We have therefore carried out simulation studies which consist of colliding an ensemble of vibrationally excited molecules [$OH(v')$ and $O_2(v'')$] having the rovibrational populations of the corresponding nascent distributions with an ensemble of oxygen molecules whose rovibrational populations mimic vibrationally cold O_2. Thus, we have replaced the multicollisional dynamics problem by a statistical-mechanics one on the basis of the quasi-ergodic theorem. The results show[19] that the final (nonequilibrium) micropopulations denoted here as "steady-state" (strictly speaking this implies nonvariation with time, a prerequisite that cannot be obviously warranted in our definition) bear a striking similarity with the initial (nascent) distributions. In fact, the largest deviations occur by far for $OH(v')$, and hence, we show only this distribution in Figure 1 (for the case of vibrationally excited oxygen, see ref 19). Clearly, the differences in the highest vibrational states manifest as a population depletion of ~30% relative to the nascent distribution. However, there is an increase in population for the states $4 \leq v' \leq 6$, while the initially empty states $0 \leq v' \leq 3$ become populated. To the extent that such distributions are representative of the true steady-state ones, the results clearly show that the latter differ drastically from Boltzmann distributions calling into question the traditional assumption of thermal equilibration in atmospheric modeling. Thus, LTD must be considered when modeling such regions of the atmosphere.

To be more specific about the transition processes occurring on the above collisions, we show in Figure 2 the probability of the vibrational transitions in the process $O_2(v'_i = 0, j'_i) + O_2(v''_i, j''_i) \rightarrow O_2(v'_f, j'_f) + O_2(v''_f, j''_f)$, where the double prime indicates the vibrationally "hot" distribution. The notable feature is perhaps the fact that transitions involving one quanta of vibrational excitation are far more favorable than those involving multiquanta jumps. In fact, one-quantum transitions are about 20−30 times more probable than two-quanta ones, and these more probable than three-quanta by roughly the same amount. Such a trend is clearly visible in a semilogarithmic fit based on the inverse exponential form

$$P(\Delta v'') = A \exp(-b|\Delta v''|) \quad (26)$$

where $A = 1.060$ (0.733) and $b = 2.773$ (2.722) are the optimum least-squares parameters for de-excitation (excitation) and

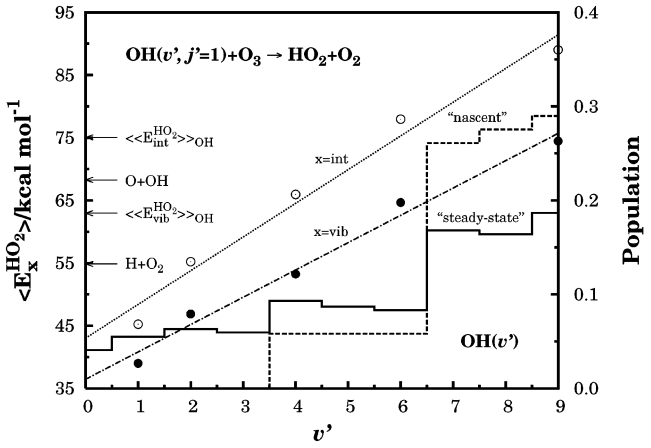

Figure 1. Average product vibrational and internal (vibrational−rotational) energies in the reaction $OH(v') + O_3 \rightarrow HO_2 + O_2$ at a collisional energy of 1 kcal mol^{-1} as a function of the OH vibrational quantum number. The dots represent the calculated[72,73] values, whereas the dotted ($\langle E_{int}^{HO_2}\rangle$/kcal mol^{-1} = 42.6 + 5.4v') and dash−dot ($\langle E_{vib}^{HO_2}\rangle$/kcal mol^{-1} = 36.3 + 4.4v') lines show straight-line fits to those points; ●, x = vib; ○, x = int. Also shown (the y axis is on the right-hand-side) is the calculated[19] steady-state vibrational distribution of OH(v'). The H + O_2 dissociation energy, and the mean vibrational ($\langle\langle E_{vib}^{HO_2}\rangle\rangle_{OH}$) and internal ($\langle\langle E_{int}^{HO_2}\rangle\rangle_{OH}$) energies of HO_2 averaged over the steady-state vibrational distribution of OH are also indicated.

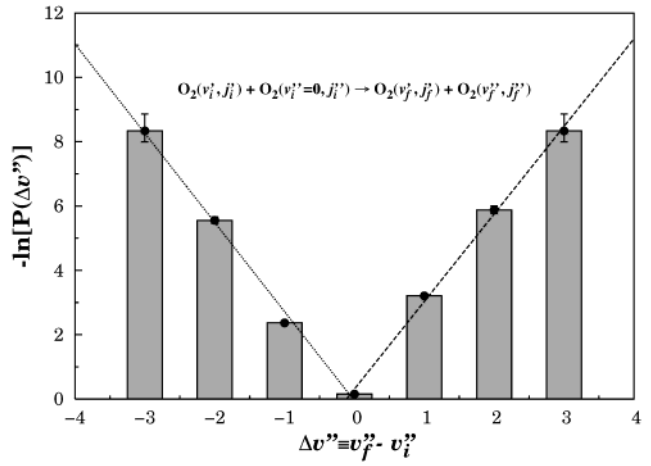

Figure 2. Logarithm of the probability of vibrational transition in the collisional process $O_2(v'_i = 0, j'_i) + O_2(v''_i, j''_i) \rightarrow O_2(v'_f, j'_f) + O_2(v''_f, j''_f)$ as a function of the multiquantum jump size. Shown by the solid dots are the computed values and corresponding error bars (hardly visible, except for the largest vibrational jumps), with the lines indicating the fits based on eq 26: (− − −) excitation; (- - -) de-excitation.

$\Delta v'' = v''_f - v''_i$ is the size of the multiquantum vibrational jump. Note that the fit has been done linearly such that low probability points are properly weighted. Despite the average high level of initial vibrational excitation, the process seems to obey well the so-called energy gap law[20,62] (describing the exponential dependence of the energy transfer probability on the energy gap) for harmonic oscillators, because $\Delta E_{vib}'' \propto \Delta v''$ where $\Delta E_{vib}'' = E_{vib,f}'' - E_{vib,i}''$. Furthermore, we observe from Figure 2 that de-excitation processes are more probable than excitation ones, as one might expect from microscopic reversibility or detailed balance.

In turn, Figure 3 shows the results obtained for the collisional process $OH(v'_i, j'_i) + O_2(v''_i = 0, j''_i) \rightarrow OH(v'_f, j'_f) + O_2(v''_f, j''_f)$, where the vibrationally hot distribution is now indicated by a single prime. Clearly, the final result contrasts

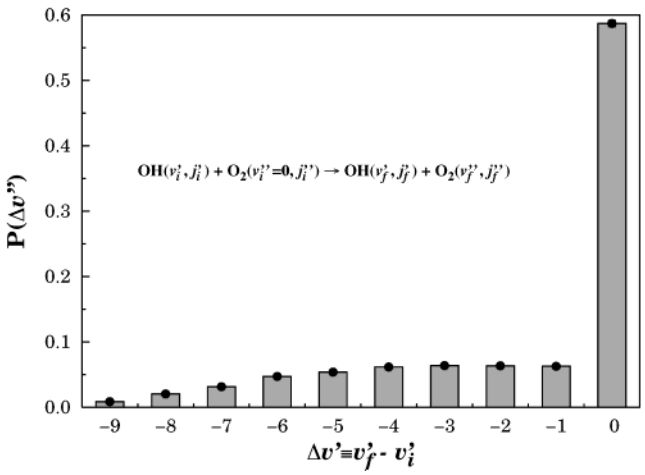

Figure 3. As in Figure 2 but for $OH(v'_i, j'_i) + O_2(v''_i = 0, j''_i) \rightarrow OH(v'_f, j'_f) + O_2(v''_f, j''_f)$.

in several respects with that obtained for the case of vibrationally excited oxygen. First, de-excitation processes are essentially the only ones observed, which may be explained from the shape of the initial vibrational distribution of OH(v'), and the relatively large size of the vibrational quanta; for the excitation process, see also ref 19. Second, multiquanta jumps occur frequently, and may involve transitions with as much as 9 vibrational quanta. Thus, it is a system far from ideal in what concerns the simple energy gap law (this has been verified only for the internal energy, because sizable errors are known to occur on its partition[63]). Although the above results may suggest that vibrational de-excitation of OH(v') in collisions with vibrationally cold O_2 is more efficient than for $O_2(v'')$, we recall from Figure 1 that the "steady-state" (nonequilibrium) micropopulation distribution of OH can still lead to an efficient production of ozone upon $OH(v') + O_2(v'')$ collisions. We further recall that dynamics studies[38] of quenching of OH(v) tend to overestimate the available experimental relaxation rates.[55,56] Although this may partly question the accuracy of the potential energy surface[64] (for an updated version of the HO_3 surface, see ref 65) used in the calculations, it also suggests that the vibrational quenching of OH may present a situation more optimistic than the results here provided seem to suggest. Of course, accurate quantum studies of vibrational quenching in $OH(v') + O_2(v'' = 0)$ collisions could help to clarify this issue. We should also emphasize that Figure 3 refers to the vibrational cooling of OH in collisions with O_2 in its vibrational ground state. However, as shown elsewhere,[37,66] it may suffice a small degree of vibrational excitation in O_2 ($v'' \geq 4$ or so) for collisions with OH($v' = 9$) to produce ozone. This may be a significant observation because, as pointed out in the Introduction, diatomic molecules such as $O_2(v'')$ near the dissociation limit are known to require 10^5-10^6 collisions to de-excite in the presence of inert species such as Ar atoms.[20] In addition, reactions involving such vibrationally excited diatomic molecules have been shown[4,37,38] to occur significantly faster than the corresponding vibrational relaxation processes, with the same being true for the reactions [photolysis of O_3, and reaction 6] through which they are produced in the middle atmosphere. Thus, vibrationally excited oxygen molecules, as well as hydroxyl radicals, should be abundant in the middle atmosphere, although only LTD modeling simulations and the solution of the involved master equations in their full complexity may allow a proper answer to the questions raised above (see sections 3.2 and 3.3).

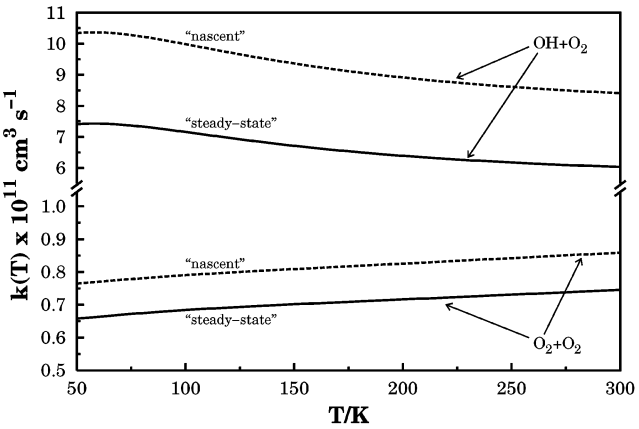

Figure 4. Total rate coefficients for odd oxygen production in $O_2(v')$ + $O_2(v'')$ and $OH(v')$ + $O_2(v'')$ reactions as a function of temperature after averaging over the nascent (dashed lines) and steady-state (solid lines) vibrational distributions of the reactant diatomics.

From the above $OH(v')$ and $O_2(v'')$ "steady-state" distributions, one can calculate the vibrationally averaged thermal rate coefficient for odd oxygen (ozone) formation. For the $OH(v')$ + $O_2(v'')$ reaction, it assumes the form

$$k^{\mathrm{odd}}(T) = \frac{\sum_{v'}\sum_{v''}\omega_{v'}\omega_{v''}k^{\mathrm{odd}}(E^{\mathrm{OH}}{}_{v',j'},E^{\mathrm{O_2}}{}_{v'',j''},T)}{\sum_{v'}\sum_{v''}\omega_{v'}\omega_{v''}} \quad (27)$$

where $k^{\mathrm{odd}}(E^{\mathrm{OH}}{}_{v',j'}, E^{\mathrm{O_2}}{}_{v'',j''}, T)$ is the specific thermal rate coefficient for odd oxygen production when the reactants have internal energies $E_{\mathrm{OH}}(v',j')$ and $E_{\mathrm{O_2}}(v'',j'')$. In the calculations reported thus far,[35,37,38,67] we have assumed $j' = 1$ and $j' = 10$, which has been shown[36] not to alter the major trends. Of course, the calculation of the specific rate coefficient for total odd oxygen production requires the evaluation of several state-specific vibrational rate constants. For the case under analysis, it is obtained as the sum of the rate coefficients for formation of HO_2 + O, O_3 + H, and O_2 + O + H plus twice the rate constant for the reaction yielding OH + O + O. Note that, for oxygen, $\omega_{v''}$ are the steady-state vibrational populations given in ref 19 (which are obtained from the 226 nm nascent distribution in the photolysis of ozone[3]), whereas $\omega_{v'}$ are the steady-state vibrational populations of $OH(v')$ referring to the experimental nascent distributions of Ohoyama et al.[21] An equivalent treatment has been adopted for the $O_2(v')$ + $O_2(v'')$ reaction, with the reader being addressed to refs 19 and 43 for details. Note that the vibrationally averaged rate constants for odd oxygen formation calculated in this way are also shown in Figure 4. For comparison, the results obtained[4] using the nascent distributions for the averaging process are also given. The differences between the two sets of estimates are seen to be typically 5% for the $O_2(v')$ + $O_2(v'')$ reaction and 30% for $OH(v')$ + $O_2(v'')$. However, the most salient feature from Figure 4 is perhaps the large magnitude of the calculated rate constants over the range of temperatures of relevance in the upper stratosphere and mesosphere, which underlines the statement made in the previous paragraph when comparing with those for vibrational quenching.

To conclude this subsection, we refer briefly to some exploratory calculations[68] that have been carried out for $O_2(v'')$ + N_2, i.e., by considering N_2 as the quencher. For this, we have added accurate diatomic curves[69] for ground-state N_2 and O_2 to an N_2-O_2 interaction potential energy surface[70] obtained from the analysis of scattering experiments and of second virial coefficient data (note that the only open channel at low collisional energies is the nonreactive N_2 + O_2 one). The results have shown an almost negligible relaxation of $O_2(v'')$ at temperatures of atmospheric interest, as one might have anticipated from the smallness of the involved vibrational−vibrational (VV) and vibrational−translational (VT) relaxation processes.[71] No similar simulation study could be done for $OH(v')$ + N_2 collisions because, to our knowledge, the relevant potential energy surface is unavailable. In summary, the major trends of the quenching of $OH(v')$ and $O_2(v'')$ obtained by using vibrationally cold O_2 as the quencher should not be drastically altered when N_2 is also considered.

3.2. Possible Implications in the HO_2/OH Partition. The $y = 1$ mechanism has been shown in section 2 to generally favor HO_2 formation over OH. Indeed, despite the fact that the reaction 6 has a rate constant nearly 3 orders of magnitude larger than (4) when OH is in its ground vibrational state, such a mechanism or the compound variant $y = (0, 1)$ should dominate at altitudes where [H] is small, thus compensating for the discrepancy in the rate constant. [At $T = 298$ K, $k_6 = 2.8 \times 10^{-11}$ cm^3 s^{-1}; for reaction 4, the values are[14,33,72] $k_{13} = 6.7 \times 10^{-14}$, 1.5×10^{-12}, 4.7×10^{-12}, and 1.7×10^{-11} cm^3 s^{-1} respectively for OH in vibrational states $v = 0$, 1, 2, and 4.] In fact, [H]/[OH] $< 10^{-2}$ up to about the stratopause,[1,9] implying from eq 15 that HO_2 formation should in principle be enhanced at this and especially higher altitudes. [This stems from the fact that vibrationally excited $OH(6 \le v \le 9)$, leading to a higher rate constant for reaction 13 is more likely to be abundant near the mesopause (85 km) where it is produced via reaction 6.] Such an expectation is in agreement with the measurements of Jucks et al.,[16] who found $[HO_2]$ at 40−50 km to be significantly larger than predicted from standard photochemical models, and with those of Sandor and Clancy[15] which extend to even higher altitudes.

The question then arises of how to explain the observation by Conway et al.[9] that the model predictions underestimate the measured OH density by about 20% at about 43 km. Clearly, the new HO_x mechanisms alone cannot explain this increase in [OH] at low altitudes[9] unless some nonconventional H sources are invoked. As we discuss in the following, a possible explanation involves vibrationally excited hydroperoxyl radicals, $HO_2(v)$, which have been denoted as $HO_2^{\star}$ in ref 73. In fact, calculations[72,73] on reaction 13 have shown that such energized hydroperoxyl radicals are largely formed with vibrational energies above the H + O_2 dissociation threshold. For example, for $OH(v' = 4)$ at a collisional energy of 0.5 kcal mol^{-1} ($T =$ 252 K), the mean vibrational (internal) energy in the products of reaction 13 is[72] $\langle E_{vib}^{\mathrm{HO_2}}\rangle = 55.9$ kcal mol^{-1} ($\langle E_{int}^{\mathrm{HO_2}}\rangle = 67.5$ kcal mol^{-1}), a value which is clearly above the classical dissociation threshold of 54.6 kcal mol^{-1}. [The rotational state of the diatomic in these calculations has been fixed at $j = 1$, although this should not offer any strong limitation for the present analysis.] If the collisional energy is 1 kcal mol^{-1}, one obtains $\langle E_{vib}^{\mathrm{HO_2}}\rangle = 53.2$ kcal mol^{-1} ($\langle E_{int}^{\mathrm{HO_2}}\rangle = 65.9$ kcal mol^{-1}), with similar or slightly larger values being predicted for higher collisional energies.[72] Indeed, by using the mean product vibrational and internal (vibrational plus rotational) energies calculated for the reaction $OH(v') + O_3 \rightarrow HO_2(v) + O_2$ at a translational energy of 1 kcal mol^{-1} and the appropriate micropopulation distribution,[19] the mean product energy of HO_2 averaged over the $OH(v')$ steady-state vibrational distribution is predicted to be $\langle\langle E_{vib}^{\mathrm{HO_2}}\rangle\rangle_{\mathrm{OH}} = 63.0$ kcal mol^{-1} ($\langle\langle E_{int}^{\mathrm{HO_2}}\rangle\rangle_{\mathrm{OH}} =$ 75.1 kcal mol^{-1}).

Figure 1 shows that $\langle\langle E_{vib}^{\mathrm{HO_2}}\rangle\rangle_{\mathrm{OH}}$ lies significantly above the classical dissociation threshold energy, leading ultimately to the

reaction $HO_2(v) \rightarrow O_2 + H$. The question is then of how much does this reaction contribute to H formation close to the stratopause. Clearly, an exact answer to this question is nontrivial. Of course, classically, all molecules with a vibrational energy above the dissociation limit would, let alone, yield $H + O_2$. However, of those molecules, a fraction collides with third bodies and eventually relax. To roughly account for this, we count as dissociative into $H + O_2$ only those molecules with an energy lying between the dissociation limit and $\langle\langle E_{vib}^{HO_2}\rangle\rangle_{OH}$. This suggests that about 13% of the energized HO_2 molecules formed via reaction 13 will produce atomic hydrogen. Of course, the HO_2 rotational energy may also contribute to this unimolecular process[74−77] [and, possibly, even allow odd oxygen formation via $HO_2(v) \rightarrow OH + O$]. In fact, if one considers the internal energy, the above fraction raises to about 28%. On the other hand, no account is being taken of the quenching of energized HO_2 due to collisions with O_2 and N_2, a study outside the scope of the present work. Because this should have an opposite effect, it is plausible to say that an average value of 20% of $HO_2(v)$ leads to H formation. Thus, one expects that 20% of the $HO_2(v)$ formed will dissociate and become a nonconventional source of H atoms, a result that shows a striking correspondence with the [OH] underestimation reported by Conway et al.[9] at 43 km. Another very significant source of hydrogen atoms comes from the direct dissociation reaction $OH(v') + O_3 \rightarrow 2O_2 + H$, which is predicted[72,73] to be very effective at high values of v'. Note that both the above processes are related via the reaction $OH(v') + O_3 \rightarrow HO_2(v) \rightarrow 2O_2 + H$, in which case the direct reaction simply implies a short-lived intermediate complex. Unless mentioned otherwise, we look at them for convenience as separate processes.

Of course, standard chemistry would predict that such nonconventionally formed H atoms would react with ozone to yield mostly vibrationally excited hydroxyl radicals, these energized HO_2, and so on. Two relevant questions then arise. The first is to know how much do such vibrationally excited hydroperoxyl radicals affect the rate of reaction 3. Although an enhancement of the corresponding thermal rate coefficient might be expected, trajectory calculations[78] have shown that such an effect is rather small even considering HO_2 with contents of vibrational excitation (this has been partioned democratically by all vibrational normal modes) close to the $H + O_2$ dissociation asymptote. Thus, it may have little implications in atmospheric modeling, especially in what concerns the specific values of the rate constants used thus far.

The second and probably most important issue refers to the partitioning of the additional HO_x species into OH and HO_2. By equating the rates of production and destruction of OH via reactions 6 and 13, one obtains

$$[OH(v')] = \frac{k_6(T)}{k_{13}(v', T)}[H] \tag{28}$$

We now recall that $OH(v')$ can be more efficiently quenched at low altitudes (note that the pressure decreases exponentially with altitude), because a wider variety of quenchers exists there. Moreover, the dominant source of $OH(v')$ in the lower mesosphere is reaction 4, which yields lower vibrational states than reaction 6. Thus, $k_6(T)$ should be considerably larger than $k_{13}(v', T)$ at such altitudes where vibrational states of OH are expected to lie closer to the ground state. Any perturbation on [H] due to the nonconventional sources should then contribute to an increase in [OH]. At higher altitudes where $6 \leq v' \leq 9$ is more likely according to the nascent distribution (this is expected to be a steady-state distribution over some period of time), one expects $k_{13}(v', T) > k_6(T)$ and hence the reverse result. Note that $k_{13}(v' = 9, T)$ can be a factor 4-fold or more larger than $k_{13}(v' = 4, T)$ [i.e., 1 order of magnitude larger than $k_6(T)$] at the temperatures of interest in the mesosphere.[4,72,73] Of course, a vertical profile of $[OH(v')]$ could help to assess the validity of our assumption, but to our knowledge, such a profile is thus far unavailable.

In an attempt to estimate the $[OH(v')]$ vertical profile and hopefully provide a quantitative model for the deficit of predicted OH density relative to observation, let us consider the following mechanism:

$$5[H + O_3 \rightarrow OH(v') + O_2] \tag{29}$$

$$3[OH(v') + O_3 \rightarrow HO_2(v) + O_2] \tag{30}$$

$$OH(v') + O_3 \rightarrow 2O_2 + H \tag{31}$$

$$OH(v') + M \rightarrow OH + M \tag{32}$$

$$OH + O_3 \rightarrow HO_2 + O_2 \tag{33}$$

$$HO_2(v) + O_3 \rightarrow OH + 2O_2 \tag{34}$$

$$HO_2(v) + M \rightarrow HO_2 + M \tag{35}$$

$$HO_2 + O_3 \rightarrow OH + 2O_2 \tag{36}$$

$$HO_2(v) \rightarrow H + O_2 \tag{37}$$

$$\text{Net:} \quad 3H + 12O_3 \rightarrow HO_2 + 16O_2 + 2OH \tag{38}$$

where reactions 31 and 37 are nonconventional sources of atomic hydrogen. By applying the stationary-state assumption to the $OH(v')$ and $HO_2(v)$ intermediate species, treated as independent, we obtain as an approximate solution for their concentrations:

$$[OH(v')]_{ss} = \frac{5k_{29}[H][O_3]}{k_{32}[M] + (3k_{30} + k_{31})[O_3]} \tag{39}$$

$$[HO_2(v)]_{ss} = \frac{15k_{29}k_{30}k_{37}[H][O_3]^2}{\{k_{32}[M] + 3(k_{30} + k_{31})[O_3]\}\{k_{37} + k_{35}[M] + k_{34}[O_3]\}} \tag{40}$$

Thus, eq 39 provides a way of estimating the dependence of $[OH(v')]$ with altitude at regions where the above mechanism prevails. For this, we carry the approximations further by assuming that the terms multiplied by [M] dominate over the others. This may be justified on the grounds that [M] exceedes $[O_3]$ by 4−5 orders of magnitude, whereas k_{30} or k_{31} are typically 2−3 orders of magnitude larger than k_{32}. One gets

$$[OH(v')]_{ss} \sim \frac{5k_{29}[H]}{k_{32}} \sim \frac{[O_3]}{[M]} \sim \frac{5k_{29}[H]}{k_{32}}[O_3]/\text{ppmv} \tag{41}$$

where $[O_3]/\text{ppmv} = [O_3]/[M]$ is the ozone mixing ratio, provided that M includes all remaining atmospheric components. A similar reasoning may be shown to yield

$$[HO_2(v)]_{ss} \sim \frac{k_{30}}{k_{35}}[OH(v')]_{ss}[O_3]/\text{ppmv} \tag{42}$$

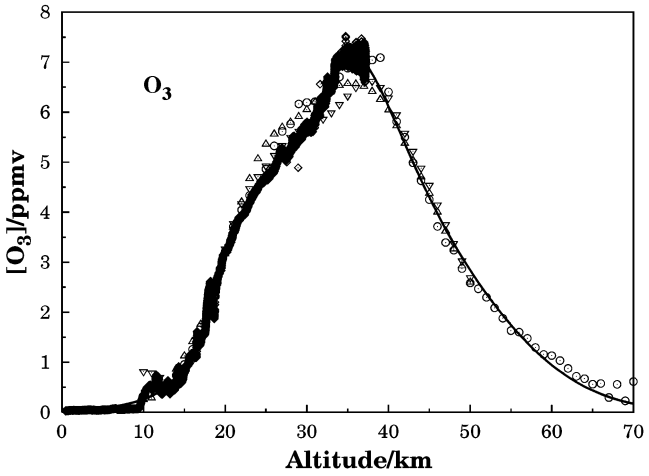

Figure 5. Balloon-borne mixing ratios of O_3 retrieved from three different instruments in a total of four curves:[80] the balloon-borne mixing ratios of [IMAGE] retrieved by FIRS-2 (△,▽), the in situ JPL O_3 photometer (◇; they show as a thick solid line disappearing after reaching the maximum due to the large number of accumulated points), and the ILAS instrument (○) on board of ADEOS.

We open here a small parenthesis to summarize the input data used for the calculations. For the ozone number density versus altitude, we have employed the SAGE (stratospheric aerosol and gas experiment) data from the vertical distribution of ozone reported by Randell et al.[79] from analyses of satelite, ground-based, and balloon measurements. Specifically, we have selected data referring to a latitude of 44° N averaged over a twelve month period, because this may be closer to the climatology associated to the MARSHI observations.[9] However, to illustrate the sensitivity of the model to variations in the input data, we have also employed an O_3 profile extracted from a traditional textbook[1] as represented by straight-line segments over appropriate altitude ranges. Similarly, we have employed O_3 mixing ratios from three different sources:[16,80] the balloon-borne mixing ratios of O_3 retrieved by FIRS-2 (far infrared spectrometer), and those obtained in situ JPL (Jet Propulsion Laboratory) O3 photometer, and from the ILAS (Improved Limb Atmospheric Sounder) instrument on board of ADEOS (Advanced Earth Observing Satellite). For the ILAS data, a more up to date and official version is included instead of the version that was available at the time ref 16 was published. In fact, the data send to us[80] amounts to four curves. Rather than using an individual set of measurements, we represented the four data sets by using the form

$$[O_3]/\text{ppmv} = \sum_{i=1}^{4} a_i \exp[-bi(z - c_i)^2] \tag{43}$$

where z is the altitude. The optimum least-squares parameters are in this case $a_1 = 4.1022$, $b_1 = 9.9246 \times 10^{-3}$, $c_1 = 32.1167$, $a_2 = 1.1197$, $b_2 = 7.7018 \times 10^{-2}$, $c_2 = 20.8959$, $a_3 = 3.9112$, $b_3 = 3.3129 \times 10^{-3}$, $c_3 = 39.2678$, $a_4 = -1.2800$, $b_4 = 7.2436 \times 10^{-2}$, and $c_4 = 30.7382$. As Figure 5 shows, the fit represents well the whole data, being especially good when used for the ILAS data alone. [The optimum parameters in eq 43 for the ILAS fit are: $a_1 = 5.5456$, $b_1 = 1.0468 \times 10^{-2}$, $c_1 = 33.3137$, $a_2 = 1.3469$, $b_2 = 5.6283 \times 10^{-2}$, $c_2 = 20.9333$, $a_3 = 3.0162$, $b_3 = 2.5594 \times 10^{-3}$, $c_3 = 40.0332$, $a_4 = -1.7940$, $b_4 = 6.8919 \times 10^{-2}$, and $c_4 = 32.6888$.] Because the results are not very sensitive to the choice of the fit, we employ only the former averaged curve in our calculations.

We now seek an answer for the ratio F^{OH} between the nonconventional [via reactions 31, 37, and 29] and conventional [via the reaction 29] rates of OH formation. First, we assume that OH is produced only via eq 29. Then we note that the rate of nonconventional OH production is identical to the rate of nonconventional H consumption and, in a stationary situation, to the rate of nonconventional H formation via reactions 31 and 37. One gets

$$F^{OH} = \frac{5}{k_{32}[M] + (3k_{30} + k_{31})[O_3]} \times \left(k_{31} + \frac{3k_{29}k_{30}}{k_{37} + k_{35}[M] + k_{34}[O_3]}\right)[O_3] \tag{44}$$

Note that k_{35} is unknown while k_{34} is unavailable but for[14,33,34] $v = \mathbf{0}$. However, it is fair to assume that k_{31} dominates in the term in parentheses due to the appearance of [M] in the denominator of the second term. If, for consistency, only k_{32}[M] is considered in the left-hand-side term, one gets

$$F^{OH} \sim \frac{5k_{31}}{k_{32}}\frac{[O_3]}{[M]} \sim \frac{5k_{31}}{k_{32}}[O_3]/\text{ppmv} \tag{45}$$

We may also define a tentative ratio for the hydroperoxyl radical, F^{HO_2}, as the quocient between the nonconventional [via reactions 30 and 35] and conventional [via reaction 33] rates of HO_2 formation, although there are further conventional sources of HO_2. After some approximations in which the terms multiplied by [M] are assumed to dominate over the others, the result assumes the form

$$F^{HO_2} \sim \frac{6k_{29}k_{30}}{k_{31}k_{33}}\frac{[H]}{[OH]}F^{OH} \tag{46}$$

For numerical purposes, it remains to specify the values of k_{29}, k_{30}, k_{31}, k_{32}, k_{35}, and [M]. Of them, k_{29} and k_{30} are well established from experiment[14] and theory,[11,13,72,73,81] whereas k_{31} can be estimated from recent calculations.[72,73,81] In turn, [M] can be extracted from the literature.[1] However, the situation is less clear for k_{32}. Two approaches have been adopted for this purpose. In the first (approach I), we have approximated the deactivation rate by

$$k_{32}[M] = \xi\left(\frac{1}{5}k_{32}^{O_2}[O_2] + \frac{4}{5}k_{32}^{N_2}[N_2]\right) \tag{47}$$

where the numerical factors account for the fact that N_2 occupies 80% of the atmosphere and ξ is a factor to be defined later. Here, we distinguish two sets of results: one is based on the O_3 profile of ref 1 (I_a) and the other employs the SAGE profile of O_3 (I_b). In approach II, we have instead defined an averaged rate constant by

$$k_{32} = \xi\left(\frac{1}{5}k_{32}^{O_2} + \frac{4}{5}k_{32}^{N_2}\right) \tag{48}$$

which may have the advantage of allowing the use of the ozone mixing ratio.[16] The situation is clearly more complicated in the case of reaction 35 because, to our knowledge, no experimental or theoretical data is available on it. Although calculations are being planned in our group on the vibrational relaxation of $HO_2(v)$, we will assume in what follows that its rate coefficient is identical to that of reaction 32.

Experimental data relative to the relaxation rate constants of $OH(v')$ in collisions with O_2 has been reported by Dodd et al.,[55] who studied the one-quantum relaxation processes $OH(v') + O_2 \rightarrow OH(v' - 1) + O_2$. For the intermediate quantum number

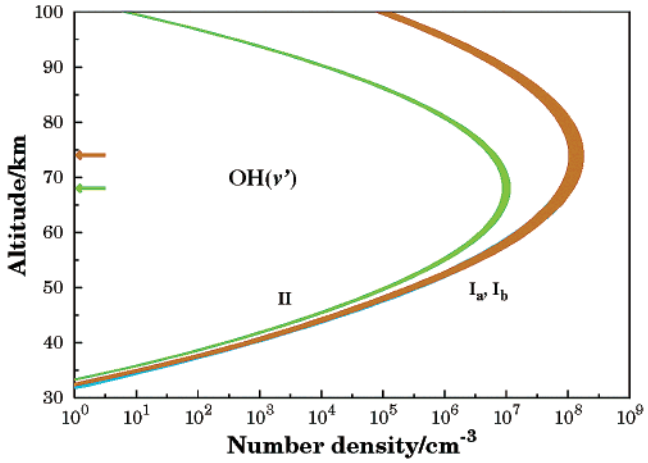

Figure 6. Dependence of [OH(v')] on altitude, as predicted from eq 41. The curves labeled I refer to the direct use of [O_3]: from ref 1 (I_a); from ref 79 (I_b). Curves II utilized the O_3 mixing ratio.[16] The colored areas delimit the [OH(v')] values calculated from the maximum and minimum values of $k_{32}^{O_2}$ and $k_{32}^{N_2}$; except over small ranges, the colored areas associated to curves I_a and I_b are nearly indistinguishable. The arrows indicate the positions of the maxima. See the text.

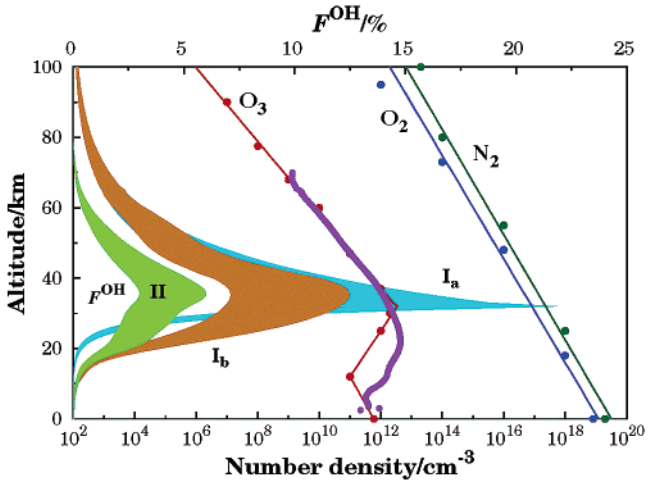

Figure 7. Dependence on altitude of [O_3], [O_2], [N_2], and ratio F^{OH} in eq 45. The data for [O_3], [O_2], and N_2 has been extracted by eye from Figure 15-2 of ref 1 and fitted by straight lines over the indicated ranges of altitude. The vertical distribution of ozone reported by Randell et al.[79] is also shown. As in Figure 6, the colored areas referring to the F^{OH}-curves I and II delimit the ratios estimated from the maximum and minimum values of $k_{32}^{O_2}$ and $k_{32}^{N_2}$. See the text.

$v' = 4$, the experimental value is[55] $k_{32}^{O_2} = (8.8 \pm 3.0) \times 10^{-13}$ cm^3 s^{-1}. However, one-quantum deexcitation processes do not necessarily imply deactivation to a level where reaction with vibrationally excited O_2 (from the ozone photolysis) can no longer occur. To obtain the rate constant for the deexcitation processes that are effective, we have to estimate the fraction of nonreactive collisions that lead to $v' < 3$, because ($v' = 3$, $v'' = 12$) is probably a conservative estimate for the combination of lowest vibrational quantum numbers of OH and O_2 capable of leading to reaction.[37] Such a fraction can be estimated from Figure 1, from which we predict $\xi = 0.095$ (this corresponds to the fractional area under the steady-state distribution for $v' \leq 2$). It is by this factor that we choose to scale the relaxation rate in eq 47 or the rate constant in eq 48. In turn, N_2 is known to be a poorer quencher of OH(v') than O_2, being established[56] that $k_{32}^{N_2} < 5 \times 10^{-13}$cm^3 s^{-1} for $v' = 9$. For a typical vibrational quantum number over the range of atmospheric interest, we may then consider as realistic the value $k_{32}^{N_2} = (10 \pm 5) \times 10^{-14}$ cm^3 s^{-1}, which should also be multiplied by ξ on the rather conservative basis that deexcitation to $v' < 3$ occurs roughly with the same probability as in collisions with O_2.

Shown by curves I_a and I_b in Figure 6 is the dependence of [OH(v')] on altitude predicted from eq 41, with the shaded areas indicating the corresponding error bars as estimated from those assigned to $k_{32}^{O_2}$ and $k_{32}^{N_2}$. [For the dependence of [H] on altitude, we have employed the following least-squares fit to the data of ref 1: $\log [H] = -17.1726 + 0.7084z - 0.0046z^2$. Similarly, we have used $[OH] = 10^7 \sum_{i=1}^{3} A_i \exp[-B_i(z - C_i)^2]$, where $A_1 = 2.7509$, $B_1 = 1.1148 \times 10^{-2}$, $C_1 = 41.3321$, $A_2 = 0.5649$, $B_2 = 6.5264 \times 10^{-3}$, $C_2 = 58.8414$, $A_3 = 0.5738$, $B_3 = 2.5385 \times 10^{-2}$, and $C_3 = 72.7239$ which represents well the data of ref 9 for $40 \leq z/\text{km} \leq 80$. Units are such that, if z is given in km, [ ] comes in cm^{-3}.] Note that [OH(v')] reaches its maximum at 68−74 km, as one would expect from the dependences on altitude of the involved number densities and the fact that reaction 16 occurs near the mesopause. Note further that predictions I_a and I_b are essentially coincident, which may be attributed to the remarkable agreement of the two O_3 number density versus altitude profiles on which they are based, while overestimating somewhat [OH(v')] based on curve II. Interestingly, its magnitude at the extreme point is $(8.5 \pm 2.3) \times 10^7$ cm^{-3}, which is in close agreement with the maximum number density reported in the literature[1] although shifted to a somewhat higher altitude. This suggests that vibrationally excited OH should be abundant in the upper mesosphere where reaction 6 actually occurs. A similar trend is observed for curve II based on the ozone mixing ratio, except that the peak emerges now at 68 km with a maximum number density of $(1.0 \pm 0.2) \times 10^7$ cm^{-3}. In this case, we have slightly enlarged the error bars to allow for an uncertainty in the O_3 mixing ratio of 10% (this has been attributed[16] to the ILAS data alone).

To calculate the ratio in eq 45, we require k_{31} which, for a typical vibrational excitation of $v = 4$, may be calculated from the data reported in previous papers[72,73] to be $k_{31} = 2.24 \times 10^{-11}$ cm^3 s^{-1}. Note that k_{31} includes the rate of formation of energized $HO_2(v)$. Figure 7 shows the calculated dependence of F^{OH} on altitude. Although the peak arises somewhere too low in altitude (~32 km) with the input data employed in method I_a, its magnitude of (17 ± 5)% is in good agreement with the observed OH surplus at 43 km, which we have hereby attributed to nonconventional H sources. The same general trend is observed in case I_b, where the corresponding values are ~ 37 km and (9.5 ± 3.0)%. Note that approach II gives a significantly lower peak of (4.5 ± 1.5)% centered at about 38 km. Note further that a close examination to Figure 2 of ref 9 shows that the MAHRSI observations leave some margin for speculation on where the peak position is located, with reasonable estimates ranging between 37 and 43 km. Moreover, the MAHRSI observations refer to a latitude of 42−58°, whereas the used ozone mixing ratios refer to northern Alaska. Because [O_3] increases on approaching the tropics, the values of F^{OH} obtained from the mixing ratios seem to be consistent with those based on the number density. In any case, our model predictions should be viewed as qualitative trends because a comparison of curves I_a and I_b near the peak shows that the calculated F^{OH} values depend somewhat on the input data used and their assigned uncertainties, some of which may be significant. A further remark to note that the H atoms produced via eq 37 should have an increasing translational energy with temperature. Because reaction 6 has a positive activation energy[14] and the temperature increases steadily from the mesopause ($T \sim 200$ K) to the stratopause ($T \sim 290$ K), one expects an enhanced

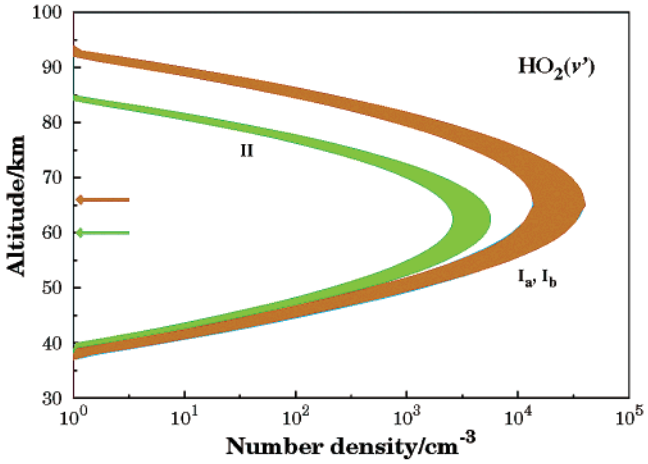

Figure 8. Dependence of $HO_2(v)$ on altitude, as predicted from eq 42. The curves are labeled following the use of the $OH(v')$ concentrations reported in Figure 6. As in Figure 6, the shaded areas delimit the minimum and maximum values of $[HO_2(v)]$, whereas the arrows indicate the positions of the maxima. See the text.

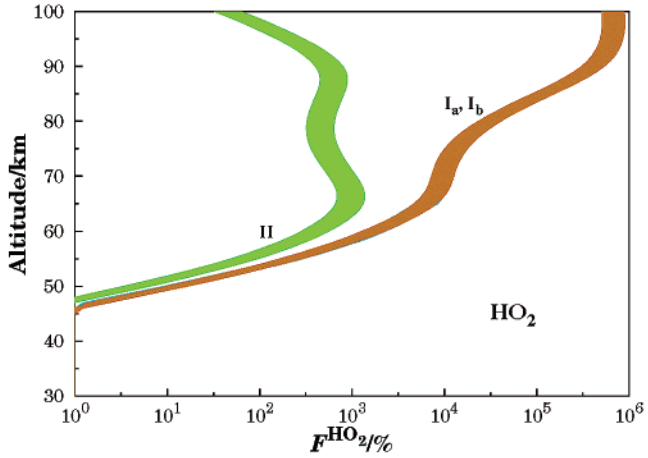

Figure 9. Dependence of F^{HO_2} on altitude, as predicted from eq 46. Notation as in Figure 7, with the colored areas delimiting the minimum and maximum values of F^{HO_2}. See the text.

$OH(v')$ formation supporting the faster growth of [OH] at 43 km or so. Note that the vertical profiles of temperature and [OH] show[9,18] a striking correlation as a function of altitude, with the temperature reversal (inversion) occurring at 50 km. Thus, we may speculate that this slight overestimation may contribute to somehow bring up the low altitudes predicted above.

We turn to Figure 8 which shows the calculated $[HO_2(v)]$ altitude profile as obtained from eq 42. The maximum occurs now at 60−66 km, thus slightly below that of $[OH(v')]$. This may be explained from the shape of the ozone mixing ratio profile which multiplies $[OH(v')]_{ss}$ in eq 42. Note that curves I_a and I_b are nearly indistinguishable, as expected from their similarity for $[OH(v')]$. Although predicted to be abundant in the mesosphere, $[HO_2(v)]$ is predicted to be up to a factor of 10^3 smaller than typical literature[1] values for total $[HO_2]$, with the peak slightly shifted to higher altitudes. The calculation of F^{HO_2} is more problematic due to uncertainties in the involved rate coefficients and number densities. For completeness, we provide the results calculated using $k_{29} = 2.8 \times 10^{-11}$ cm^3 s^{-1}, $k_{30} = 1.7 \times 10^{-11}$ cm^3 s^{-1}, $k_{31} = 2.24 \times 10^{-11}$ cm^3 s^{-1}, and $k_{33} = 1.7 \times 10^{-11}$ cm^3 s^{-1}. Of these, k_{31} has been used in the calculation of F^{OH}, whereas k_{29} has a well-established value.[14] In turn, we have assumed $k_{33} = k_{30}$ with the value of k_{30} corresponding[72] to $T = 300$ K and $OH(v = 4)$. This may be justified on the grounds that, for $v \leq 4$, the product HO_2 has an average vibrational content smaller than the $H + O_2$ dissociation energy (see Figure 1), although it may possibly lead to some underestimation of F^{HO_2}. This is shown in Figure 9 for altitudes $z \leq 100$ km. A few points deserve attention. First, we should note that the fit of [OH] versus z is, strictly speaking, reliable only up to 80 km. The results shown for $80 \leq z/\text{km} \leq 100$ have therefore been included only to illustrate the sensitivity of the model to the input number densities. They suggest that the values of F^{HO_2} calculated from F^{OH} obtained from the ozone mixing ratio may have the advantage of partly anihilating the errors which occur when [H] and [OH] are extrapolated to altitudes above 80 km. Second, for altitudes above 50 km, the new mechanisms predict a marked increase in $[HO_2]$ relative to the standard values obtained via reaction 33. Third, the nonconventional mechanisms are most efficient at 65 km and even higher altitudes where a significant fraction of HO_2 radicals should be highly vibrationally excited and possibly in route to $H + O_2$ dissociation. Finally, the novel mechanisms are found to predict additional $[HO_2]$ values of up to 100% at 50−55 km in qualitative agreement with the observed trends,[15,16] although they have no impact at regions where the peak in F^{OH} arises.

3.3. Possible Implications on O_3 Production. The possible effect on the concentrations of O_3 and HO_2 can only be reliably assessed by atmospheric modeling using, in principle, all atmospheric constituents within LTD. Obviously, such a task would be overwhelming given the numerous state-specific reaction rate constants that are required for each atmospheric constituent. A simplified approach that proved satisfactory in the case of a pure-oxygen atmosphere[3] consists of using the stationary-state assumption. For the $y = (0, 1)$ mechanism, it leads to the following fractional additional odd oxygen production relative to the rate of O_3 production in the conventional mechanism:

$$F_{01}^{O_3} = \left\{\frac{k}{k_D}\left(2R_{v'' \geq v''_0} R_{\lambda_0} J_{O_3 \rightarrow O(^3P)} + \frac{3}{2} k_{16}[H]\right) + 2\left(\frac{k_{22}}{k'_D} - \frac{k}{4k_D}\right) k_{17}[OH]\right\} \frac{[O_3]}{8 J_{O_2}[O_2]} \quad (49)$$

where k_D and k_D' are the total collisional removal rates of $OH(v')$ and $O_2(v'')$ and $k = k_{19} + k_{20} + 2k_{21}$ is the total rate constant for odd oxygen formation in reactions 19 to 21; k_n is the rate constant of reaction (n), and the factor 2 in k accounts for the fact that two oxygen atoms are produced in eq 21. Note that a constant yield $\Phi_{v'' \geq v''_0}(\lambda) = \Phi R_{v'' \geq v''_0}$ [Φ is the quantum yield of reaction $O_3 + h\nu \rightarrow O_2 + O(^3P)$ for production of O_2 in a state $v'' \geq v''_0$, and $R_{v'' \geq v''_0}$ is the probability for such a reaction to produce such high vibrational states] has been assumed,[3] $R_{\lambda_0} = \int_{\lambda < \lambda_0} J_{O_3}(\lambda, z, \chi)\, d\lambda / \int J_{O_3}(\lambda, z, \chi)\, d\lambda$ is the fraction of O_3 photolysis which takes place at wavelengths shorther than λ_0, and $J_{O_3 \rightarrow O(^3P)} = \Phi \int_{\lambda < \lambda_0} J_{O_3}(\lambda, z, \chi)\, d\lambda$ is the total O_3 photolysis rate constant leading to $O(^3P)$. Note also that eq 49 differs from eq 30 of ref 19 in that we have neglected the second term in curly brackets due to its small magnitude at stratospheric temperatures. Note especially that the wavelength integrated photolysis rate of O_2 is $2J_{O_2}[O_2]$ per photon, and hence a dividing factor of 4 has been considered to account for the four photons consumed in the $y = (0, 1)$ mechanism, eqs 16−23.

For simplicity, we will assume that $k \sim k_D$ and $k_{22} \sim k'_D$. We therefore ignore the inelastic processes, which should not have a drastic effect since the corresponding rate constants have been shown[37] to be a factor of 5 or so smaller than the reactive

ones. We further assume the O_3 photolysis to be at $\lambda = 226$ nm, $v''_0 = 26$, $R_{v''\geq 26} = 0.081$, and the long wavelength threshold for production of vibrationally excited O_2 to be $\lambda_0 = 243$ nm, because these data can be taken directly from ref 3. Because a good guess for the lowest vibrational quantum numbers capable of leading to reaction is[37] ($v' = 3$, $v'' = 12$), our estimates for the fraccional additional odd oxygen production relative to the rate of O_3 production in the conventional mechanism may therefore be viewed as conservative because other wavelengths can concur to production of vibrationally excited O_2. Despite this, the $y = (0, 1)$ mechanism yields O_3 at rates that range from 0.1 to about 3 the principle O_2 photodissociation source as the altitude varies from 40 to 55 km. These values differ slightly from those reported elsewhere[19] due to the different sources employed for the input data, in particular $[O_2]$. Moreover, to extend the calculations beyond 55 km, we have employed the following representations: $10^{10}J_{O_2}/s^{-1} = -1.493 + 0.468h$, $J_{O_3\rightarrow O(^3P)}/s^{-1} = -0.068 + 0.0038h$, and $R_{\lambda_0} = -0.068 + 0.0038h$, whereas the dependence of T on altitude has been modeled by straight-line segments as suggested in Figure 2.1 of ref 82. A similar analysis for $F_{12}^{O_3}$ reveals that this is considerably smaller than the Wodtke ratio over the same range of altitudes. Thus, $F_{01}^{O_3}$ dominates at high altitudes where atomic hydrogen plays an increasing role: it is three times smaller than Wodtke's ratio[3] at 40 km but becomes 20 times larger or so at 55 km! Parenthetically, we should note that Wodtke's analysis[3] may be too simplistic in that he assumes that, for $v = 26$, reaction 7 proceeds instantly and completely. However, it provides useful data that will be used here for the sake of comparison. Note that a computer simulation[3] based on a radiative-transport-chemical model which included reaction 25 has predicted the percentage difference between a model with and without that reaction to display a maximum increase of 10% at an altitude of about 43 km. After reaching the maximum, the predicted efficiency for O_3 production is considerably reduced,[3] with the model failing to ameliorate the ozone deficit problem. In fact, a more recent analysis has shown[83] that such a model cannot account for the deficit at higher altitudes even if all $O_2(v)$ leads to production of ozone via a reaction similar to (25).

In an attempt to be as realistic as possible, we now try to account for the collisions with N_2 that have been ignored thus far. Because N_2 occupies 80% of the atmosphere, the question is whether a collision of $OH(v')$ with nitrogen can leave OH sufficiently hot to react with $O_2(v'')$. Measurements have shown[56] that N_2 is a slow collider leading to a slow decrease in the population of $OH(v = 9)$. The remaining 20% probability refers therefore to collisions of $OH(v')$ with molecular oxygen. Although this has been found[56] to be the dominant quencher, the nascent (steady-state) distribution suggests that the chance of such collisions to involve an $O_2(v'')$ that would lead to odd oxygen formation is 12% (13%), 8% (10%), and 4% (5%) when $v''_0 = 24$, 25, and 26, respectively. Note, however, that these values are considerably larger than the estimated threshold quantum number of $v''_0 = 13$, and hence would lead to very conservative estimates in the present analysis. A more reasonable value may indeed be to consider the probability associated to values close to $v''_0 = 13$. This has an associated probability of 65%, a value that reduces to 43% and 37% if one assumes instead $v''_0 = 16$ and 17, respectively. Thus, we proceed the analysis by considering an estimated probability of roughly 40%.

Naturally, one should also bear in mind that there is a threshold vibrational state[37] of OH for forming O_3 in collisions with $O_2(v'' \geq v''_0)$, namely $v'_0 \geq 3$. As it can be seen from Figure 1 by looking to the area under the steady-state vibrational distribution, the probability of encountering such an OH species is ~90%. From this and the above probabilities, one obtains a composite probability of ~8% (as obtained from $0.2 \times 0.4 \times 0.9$) for a successful reactive encounter leading to ozone formation. Both $F_{01}^{O_3}$ and $F_{02}^{O_3}$ are accordingly scaled down by a factor of 8/100, yielding the ratios actually shown in Figure 10 as a function of altitude. We emphasize that $F_{01}^{O_3}$ remains nearly twice the Wodtke ratio at 55 km where the latter is unable to account for the known "ozone deficit problem".[3] In fact, even $F_{02}^{O_3}$ is at the level of Wodtke's ratio at 55 km, although about twice smaller than for $y = (0, 1)$ due to the lower efficiency of the photons used to sustain the less reactive processes.[19] Finally, both $F_{01}^{O_3}$ and $F_{02}^{O_3}$ predict a maximum near 70 km which may be explained from the dependence of [H] on altitude. Needless to say, some scaling of the experimental rate constants within their error limits remains a valid procedure.

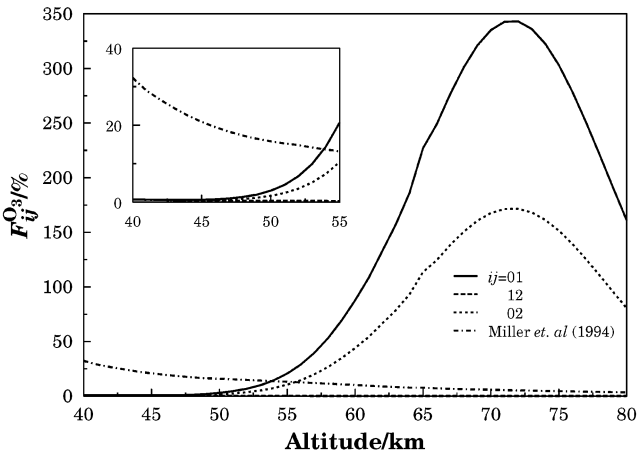

Figure 10. Comparison of the $F_{ij}^{O_3}$ (ij = 01, 12, 02) ratios (down-scaled by 8/100) for the new HO_x mechanisms with the Wodtke[3] O_x results obtained from the input data used in the present work. The small bump at about 65 km is due to passing from the vertical distribution of ozone reported by Randell et al.[79] to the linear fit as shown in Figure 7. Except in the insert, $F_{12}^{O_3}$ is invisible within the scale of the figure.

4. Concluding Remarks

The O_x mechanism of Wodtke and co-workers[3] and our own[4] revision of it together with the novel HO_x mechanisms from the present work, although somewhat hypothetical, suggest a clue to explain the "ozone deficit problem" both in the stratosphere and mesosphere. Such HO_x mechanisms, jointly with reactions 31 and 37, have been shown to simultaneously help to unfold the "HO_x dilemma".

We emphasize three points related to the novel mechanisms of the present work. First, they find support on consistent theoretical studies[4,11,19,35−38,72,73,81] of the involved elementary chemical reactions. In fact, the rate coefficients for some reactions involving vibrationally excited OH and O_2 were even taken from trajectory calculations carried out for such reactions. Although these neglect quantum effects (which may play an important role at temperatures of relevance in the middle atmosphere) and rely on potential energy surfaces that are certainly not free from innaccuracies, good agreement with experiment has been observed for the corresponding reverse reactions giving confidence on the predictions made. Thus, although we believe that upgrading theory at the level of the involved elementary chemical reactions may not lead to drastic changes in the major trends reported in the present work, the species involved possess an open shell electronic structure and

hence the effect of nonadiabaticity in describing their collision dynamics remains an open issue. The second point refers to reactions 31 and 37. If they occur in the atmosphere, they could possibly have an effect on the [H] altitude profile. This could eventually be seen by comparing actual observations with standard model simulations as an H deficit. Alternatively, model simulations with their inclusion and without their consideration could help to study their impact. To our knowledge, no manifestation of an atomic hydrogen deficit has so far been observed. We emphasize though that LTD atmospheric modeling is essential if the quantitative details of our predictions are to be established. The third and final point to note that atmospheric models often incorporate hundreds of chemical reactions, measured distributions of long-lived species (which depend more on transport processes than on chemistry), and solar ilumination (which influences the chemical composition of the atmosphere through hundreds of photochemical reactions), and hence the analysis of the present work may have the merit of simplicity in helping to unravel the title problems.

Acknowledgment. The author thanks Ken Jucks (Harvard-Smithsonian Center for Astrophysics, Cambridge, Massachusetts, U.S.A.) for providing the data on the ozone mixing ratios and William Randel and Fei Wu (Atmospheric Chemistry Division, National Center for Atmospheric Research, Boulder, U.S.A.) for providing the number density versus altitude ozone profiles. This work has the financial support of Fundação para a Ciência e a Tecnologia, Portugal, via program POCTI/40154/QUI/2001. The partial support from FEDER is also gratefully acknowledged.

References and Notes

(1) Steinfeld, J. I.; Francisco, J. S.; Hase, W. L. *Chemical Kinetics and Dynamics*; Prentice Hall: Englewood Cliffs, NJ, 1989.
(2) Wayne, R. P. *Chemistry of Atmospheres*, 3rd ed.; Oxford University Press: Oxford, 2002.
(3) Miller, R. L.; Suits, A. G.; Houston, P. L.; Toumi, R.; Mack, J. A.; Wodtke, A. M. *Science* **1994**, *265*, 1831.
(4) Varandas, A. J. C. *ChemPhysChem* **2002**, *3*, 433.
(5) Crutzen, P. J.; Grooss, J. U.; Brühl, C.; Müller, R.; Russell, J. M., III. *Science* **1995**, *268*, 705.
(6) Osterman, G. B.; Salawitch, R. J.; Sen, B.; Toon, G. C.; Stachnik, R. A.; Pickett, H. M.; Margitan, J. J.; Blavier, J.; Peterson, D. B. *Geophys. Res. Lett.* **1997**, *24*, 1107.
(7) Eluszkiewicz, M. A. J.; Allen, M. *J. Geophys. Res.* **1993**, *98*, 1069.
(8) Clancy, R. T.; Rusch, D. W.; Thomas, R. J.; Allen, M.; Eckman, R. S. *J. Geophys. Res.* **1987**, *92*, 3067.
(9) Conway, R. R.; Summers, M. E.; Stevens, M. H.; Cardon, J. G.; Preusse, P.; Offermann, D. *Geophys. Res. Lett.* **2000**, *27*, 2613.
(10) Summers, M. E.; Conway, R. R.; Siskind, D. E.; Stevens, M. H.; Offermann, D.; Riese, M.; Preusse, P.; Strobel, D. F.; Russell, J. M., III. *Science* **1997**, *277*, 1967.
(11) Varandas, A. J. C. *Int. Rev. Phys. Chem.* **2000**, *19*, 199.
(12) Setokuchi, O.; Sato, M.; Matuzawa, S. *J. Phys. Chem. A* **2000**, *104*, 3204.
(13) Fernández-Ramos, A.; Varandas, A. J. C. *J. Phys. Chem. A* **2002**, *106*, 4077.
(14) Atkinson, R.; Baulch, D. L.; Cox, R. A.; Hampson, Jr., R. F.; Kerr, J. A.; Rossi, M. J.; Troe, J. *J. Phys. Chem. Ref. Data* **1997**, *26*, 521.
(15) Sandor, B. J.; Clancy, R. T. *J. Geophys. Res.* **1998**, *103*, 13337.
(16) Jucks, K. W.; Johnson, D. G.; Chance, K. V.; Traub, W. A.; Margitan, J. J.; Osterman, G. B.; Salavitch, R. J.; Sasano, Y. *Geophys. Res. Lett.* **1998**, *25*, 3935.
(17) Pickett, H. M.; Peterson, D. B. *J. Geophys. Res.* **1996**, *101*, 16789.
(18) Day, C. *Phys. Today* **2000**, (November), 17.
(19) Varandas, A. J. C. *J. Phys. Chem. A* **2003**, *107*, 3769.
(20) Teitelbaum, H. *Chem. Phys.* **1988**, *124*, 55.
(21) Ohoyama, H.; Kasai, T.; Yoshimura, Y.; Kuwata, H. *Chem. Phys. Lett.* **1985**, *118*, 263.
(22) Jongma, R. T.; Shi, S.; Wodtke, A. M. *J. Chem. Phys.* **1999**, *111*, 2588.
(23) Hernández-Lamoneda, R.; Hernández, M. I.; Campos-Martínez, J. *Chem. Phys. Lett.* **2003**, *368*, 709.
(24) Walch, S. P.; Duchovic, R. J. *J. Chem. Phys.* **1992**, *96*, 4050.
(25) Walch, S. P.; Duchovic, R. J. *J. Chem. Phys.* **1991**, *94*, 7068.
(26) Kendrick, B. K.; Pack, R. T *J. Chem. Phys.* **1995**, *102*, 1994.
(27) Varandas, A. J. C.; Voronin, A. I. *J. Phys. Chem.* **1995**, *99*, 15846.
(28) Kupperman, A. In *Dynamics of Molecules and Chemical Reactions*; Wyatt, R. E., Zhang, J. Z. H., Eds.; Marcel, Dekker: New York, 1996; p 411.
(29) Kendrick, B. K.; Pack, R. T *J. Chem. Phys.* **1997**, *106*, 3519.
(30) Yarkony, D. R. *J. Phys. Chem. A* **2001**, *105*, 6277.
(31) Varandas, A. J. C.; Xu, Z. R. In *Advances in Chemical Physics*; Baer, M., Billing, G. D., Eds.; Wiley: New York, 2002; Vol. 124, p 659.
(32) Varandas, A. J. C. In *Fundamental World of Quantum Chemistry: A Tribute Volume to the Memory of Per-Olov Löwdin*; Brändas, E. J., Kryachko, E. S., Eds.; Kluwer: Dordrecht, The Netherlands, p 33; Vol. 2, Chapter 2.
(33) Steinfeld, J. I.; Adler-Golden, S. M.; Gallagher, J. W. *J. Phys. Chem. Ref. Data* **1987**, *16*, 911.
(34) Herndon, S. C.; Villata, P. W.; Jayne, J. T.; Zahniser, M. S. *J. Phys. Chem. A* **2001**, *105*, 1583.
(35) Caridade, P. J. S. B.; Betancourt, M.; Garrido, J. D.; Varandas, A. J. C. *J. Phys. Chem. A* **2001**, *105*, 7435.
(36) Varandas, A. J. C.; Caridade, P. J. S. B. *Chem. Phys. Lett.* **2001**, *339*, 1.
(37) Garrido, J. D.; Caridade, P. J. S. B.; Varandas, A. J. C. *J. Phys. Chem. A* **2002**, *106*, 5314.
(38) Caridade, P. J. S. B.; Sabin, J.; Garrido, J. D.; Varandas, A. J. C. *Phys. Chem. Chem. Phys.* **2002**, *4*, 4959.
(39) Price, J. M.; Mack, J. A.; Rogaski, C. A.; Wodtke, A. M. *Chem. Phys.* **1993**, *175*, 83.
(40) Rogaski, C. A.; Mack, J. A.; Wodtke, A. M. *Faraday Discuss.* **1995**, *100*, 229.
(41) Hernández-Lamoneda, R.; Toumi, R.; Clary, D. C. *J. Chem. Phys.* **1995**, *102*, 9544.
(42) Balakrishnan, N.; Billing, G. D. *Chem. Phys. Lett.* **1995**, *242*, 68.
(43) Varandas, A. J. C.; Wang, W. *Chem. Phys.* **1997**, *215*, 167.
(44) Hernández-Lamoneda, R.; Hernández, M. I.; Carmona-Novillo, E.; Campos-Martínez, J.; Echave, J.; Clary, D. C. *Chem. Phys. Lett.* **1997**, *276*, 152.
(45) Wang, W.; Varandas, A. J. C. *Chem. Phys.* **1998**, *236*, 181.
(46) Campos-Martínez, J.; Carmona-Novillo, E.; Echave, J.; Hernández, M. I.; Hernández-Lamoneda, R.; Palma, J. *Chem. Phys. Lett.* **1998**, *289*, 150.
(47) Lauvergnat, D.; Clary, D. *J. Chem. Phys.* **1998**, *108*, 3566.
(48) Balakrishnan, N.; Dalgarno, A.; Billing, G. D. *Chem. Phys. Lett.* **1998**, *288*, 657.
(49) Hernández-Lamoneda, R.; Ramírez-Solis, A. *J. Chem. Phys.* **2000**, *113*, 4139.
(50) Varandas, A. J. C.; Pais, A. A. C. C. In *Theoretical and Computational Models for Organic Chemistry*; Formosinho, S., Czismadia, I., Arnaut, L., Eds.; Kluwer: Dordrecht, The Netherlands, 1991; p 55.
(51) Varandas, A. J. C. *Adv. Chem. Phys.* **1988**, *74*, 255.
(52) Varandas, A. J. C. In *Lecture Notes in Chemistry*; Laganá, A., Riganelli, A., Eds.; Springer: Berlin, 2000; Vol. 75, p 33.
(53) Varandas, A. J. C. In *Conical Intersections: Electronic Structure, Dynamics and Spectroscopy*; Yarkony, D., Köppel, H., Domcke, W., Eds.; World Scientific Publishing: Singapore, 2003.
(54) Sappey, A. D.; Copeland, R. A. *J. Chem. Phys.* **1990**, *93*, 5741.
(55) Dodd, J. A.; Lipson, S. J.; Blumberg, W. A. M. *J. Chem. Phys.* **1991**, *95*, 5752.
(56) Chalamala, B. R.; Copeland, R. A. *J. Chem. Phys.* **1993**, *99*, 5807.
(57) Parker, H.; Slanger, T. G. *J. Chem. Phys.* **1994**, *100*, 287.
(58) Mack, J. A.; Mikulecky, K.; Wodtke, A. M. *J. Chem. Phys.* **1996**, *105*, 4105.
(59) Knutsen, K.; Dyer, M. J.; Copeland, R. A. *J. Chem. Phys.* **1996**, *104*, 5798.
(60) Hickson, K. M.; Sharkey, P.; Smith, I. W. M.; Symonds, A. C.; Tuckett, R. P.; Ward, G. N. *Phys. Chem. Chem. Phys.* **1998**, *94*, 533.
(61) Slanger, T. G.; Jusinski, L. E.; Black, G.; Gadd, G. E. *Science* **1988**, *241*, 945.
(62) Forst, W.; Penner, A. P. *J. Chem. Phys.* **1980**, *72*, 1435.
(63) Varandas, A. J. C.; Llanio-Trujillo, J. L. *J. Theor. Comput. Chem.* **2002**, *1*, 31.
(64) Varandas, A. J. C.; Yu, H. G. *Mol. Phys.* **1997**, *91*, 301.
(65) Yu, H. G.; Varandas, A. J. C. *Chem. Phys. Lett.* **2001**, *334*, 173.
(66) Caridade, P. J. S. B.; Zhang, L.; Garrido, J. D.; Varandas, A. J. C. *J. Phys. Chem. A* **2001**, *105*, 4395.
(67) Garrido, J. D.; Caridade, P. J. S. B.; Varandas, A. J. C. *J. Phys. Chem.* **1999**, *103*, 4815.
(68) Varandas, A. J. C.; Caridade, P. J. S. B. Unpublished work.
(69) Varandas, A. J. C.; Silva, J. D. *J. Chem. Soc., Faraday Trans.* **1992**, *88*, 941.
(70) Aquilanti, V.; Bartolomei, M.; Cappelletti, D.; Carmona-Novillo, E.; Pirani, F. *Phys. Chem. Chem. Phys.* **2001**, *3*, 3891.
(71) Billing, G. D. *Chem. Phys.* **1994**, *179*, 463.

(72) Zhang, L.; Varandas, A. J. C. *Phys. Chem. Chem. Phys.* **2001**, *3*, 1439.
(73) Varandas, A. J. C.; Zhang, L. *Chem. Phys. Lett.* **2001**, *340*, 62.
(74) Dobbyn, A. J.; Stumpf, M.; Keller, H.-M.; Hase, W. L.; Shinke, R. *J. Chem. Phys.* **1995**, *103*, 9947.
(75) Dobbyn, A. J.; Stumpf, M.; Keller, H.-M.; Schinke, R. *J. Chem. Phys.* **1996**, *104*, 8357.
(76) Marques, J. M. C.; Varandas, A. J. C. *J. Phys. Chem.* **1997**, *101*, 5168.
(77) Marques, J. M. C.; Llanio-Trujillo, J. L.; Varandas, A. J. C. *Phys. Chem. Chem. Phys.* **2000**, *2*, 3583.
(78) Silveira, D. M.; Caridade, P. J. S. B.; Varandas, A. J. C. To be published.
(79) Randel, W. J.; Stolarski, R. S.; Cunnold, D. M.; Logan, J. A.; Newchurch, M. J.; Zawodny, J. M. *Science* **1999**, *285*, 1689.
(80) Jucks, K. W. Private communication, June 2003.
(81) Varandas, A. J. C.; Zhang, L. *Chem. Phys. Lett.* **2000**, *331*, 474.
(82) van Loon, G. W.; Duffy, S. J. *Environmental Chemistry. A Global Perspective*; Oxford University Press: Oxford, 2002.
(83) Geiser, J.; Dylewski, S. M.; Mueller, J. A.; Wilson, R. J.; Toumi, R.; Houston, P. L. *J. Chem. Phys.* **2000**, *112*, 1279.